


## Crystal Polymorphism Induced by Surface Tension

Cédric Schoonen<sup>1</sup> and James F. Lutsko<sup>1\*</sup>

Center for Nonlinear Phenomena and Complex Systems CP 231, Université Libre de Bruxelles,  
Boulevard du Triomphe, 1050 Brussels, Belgium

 (Received 20 June 2022; revised 7 September 2022; accepted 10 November 2022; published 7 December 2022)

We use classical density functional theory (cDFT) to calculate fluid-solid surface tensions for fcc and bcc crystals formed by hard spheres and Lennard-Jones (LJ) particles. For hard spheres, our results show that the recently introduced “explicitly stable” functionals perform as well as the state of the art, and for both interaction potentials, our results compare well to simulation. We use the resulting bulk and interfacial energies for LJ to parametrize a capillary model for the free energy of small solid clusters and thereby determine the relative stability of bcc and fcc LJ clusters. We show a crossover from bcc to fcc stability as cluster size increases, thus providing insight into long-standing tension between simulation results and theoretical expectations. We also confirm that the bcc phase in contact with a vapor is unstable, thus extending earlier zero-temperature results. Our Letter demonstrates the potential of cDFT as an important tool in understanding crystallization and polymorphism.

DOI: [10.1103/PhysRevLett.129.246101](https://doi.org/10.1103/PhysRevLett.129.246101)

**Introduction.**—Crystallization is a complex phenomenon that is central to numerous physical, biological, and technological applications (see, e.g., Kashchiev [1] for a wide-ranging general discussion). It may involve the direct formation of the crystal from the mother phase, usually referred to as the classical nucleation, or via multiple steps involving one or more other phases such as vapor to droplets to crystals, usually called nonclassical nucleation [2,3]. Importantly, crystals involve discrete spatial symmetries and the same substance can often form solids with different crystal symmetries, i.e., different polymorphs, and one polymorph can transform to another. Control of polymorphism is a critical practical problem, notably in the production of pharmaceuticals [4–7].

Crystallization begins with the formation of small clusters and the preference for different polymorphs depends on their relative free energies (as well as on separate kinetic factors). The free energies of clusters is often thought of in terms of the free energy of the bulk-phase interior and the surface free energy (or surface tension). While the former is quite accessible, determining solid-fluid surface tensions is challenging, even using simulations [8,9]. An alternative to direct simulation is classical density functional theory (cDFT) [10,11] which offers a unique approach to probing interfacial properties. As a theoretical technique that includes fluctuations intrinsically, it gives access to statistical properties without the noise inherent in simulations and thus offers a useful complementary *ab initio* approach. Recent years have seen the maturation of cDFT into a tool which can provide such information with quantitative accuracy in comparison to simulations [9,12,13].

Here, we report the calculation of bulk and surface properties calculated using highly accurate cDFT models

and use the results to model the thermodynamics of small crystalline polymorphs in a Lennard-Jones (LJ) system. We use these models to address the long-standing tension between the landmark paper of Alexander and McTague [14] suggesting, based on very general Landau-model arguments, that all crystallization should favor bcc clusters, and the subsequent failure of simulation to confirm this prediction (see, e.g., Swope and Andersen [15]). Our results are consistent with the simulations of ten Wolde *et al.* [16] and of Desgranges and Delhomelle [17] suggesting that bcc may well be favored for very small, subcritical clusters but that a crossover occurs after which fcc is favored and we predict such a crossover for clusters of a few hundred atoms at most.

**Theory.**—Classical DFT is a reformulation of some aspects of equilibrium statistical mechanics [10,11]. As in quantum DFT, the primary actor is the local number density  $\rho(\mathbf{r})$ , which is the same as the one-body distribution function and exact theorems assert the existence of a functional of the local density which, upon minimization, gives the equilibrium density distribution and the total grand-canonical free energy  $\Omega$ . In general, the exact functional is not known, and calculations are based on models designed to satisfy various exact limits.

The present Letter is based on the recently developed “explicitly stable fundamental measure theory” (esFMT) model [13] for hard spheres. For calculations involving spherically symmetric pair potentials like the LJ potential, we use the usual cDFT paradigm of writing the functional as a hard-sphere contribution (using esFMT) and a mean-field term accounting for long-ranged attractions (see Ref. [18] and the companion paper [19] for details). These expressions are evaluated on a cubic computational

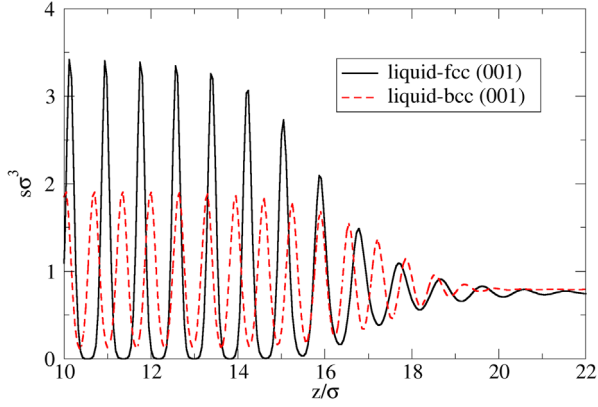


FIG. 1. Solid-liquid interfaces for both bcc and fcc Lennard-Jones solids (001) planes as determined from cDFT. The temperature is  $k_B T = 1.0\epsilon$ , where  $\epsilon$  is the LJ energy scale and the lengths are scaled to  $\sigma$ , the LJ length scale which is the typical size of an atom or molecule. The figure shows the planar densities  $s(z)$ , which are the densities averaged over the planes perpendicular to the interface.

lattice (not to be confused with the crystal lattice) following Refs. [18,20] and minimized using the FIRE2 algorithm [21]. Unless otherwise stated, we used a lattice spacing of about 0.05 molecular diameters throughout this Letter.

To determine the interfacial free energy between two phases, we work with a slab geometry with the  $z$  axis normal to the interfaces. The size of the computational cell in the  $x$ - $y$  directions is determined by the dimensions of the unit cell of the solid, while in the  $z$  direction, the length is approximately 50 molecular diameters giving on the order of 25 lattice planes of solid. By way of illustrating the results, Fig. 1 shows the planar densities for equilibrated fcc-liquid and bcc-liquid interfaces for a LJ system. A characteristic difference between the bcc and fcc structures is that the distribution of density around the Bravais lattice points has smaller amplitude and is broader for bcc than for fcc reflecting the less-closely packed nature of the former, as can be seen in the planar densities as well. The interface between the solid and liquid includes 7 or 8 lattice planes

for bcc giving an interfacial width of about 5 molecular diameters and about 10 lattice planes for fcc giving a width of around 9 diameters.

We calculated the surface tension by introducing a Gibbs dividing surface (see Supplemental Material [22] for details). Table I shows our results for hard spheres using both the state-of-the-art White Bear II (WBII) functional, including for comparison previous calculations [25] and the esFMT. Our methods are validated by the agreement with previous work and show that the results using both cDFT functionals are of similar quality compared to simulation, with the difference however that the esFMT results are generally lower than the simulation values whereas the WBII results are higher. Qualitatively, the ordering  $\gamma_{(111)} < \gamma_{(110)} < \gamma_{(001)}$  of fcc crystal faces according to the interfacial free energy is consistent in all cases considered. Quantitatively, the difference of 10%–20% between cDFT and simulation results should be contrasted with the significant variation between simulation results recently reported in the literature, which is at least half this range.

Table I also shows results for bcc-fluid interfaces and the only prior results we are aware of, also cDFT calculations using the WBII functional. As for the fcc phase, the esFMT surface tensions are systematically smaller than those determined using WBII and are, in both cases, about half the surface tension for the fcc interface. Despite the well-known fact that the bcc phase of hard spheres is unstable to shear [27], we find no sign of an instability in the bcc in contact with the fluid phase [19].

*Interfacial properties of the Lennard-Jones solid.*—Our calculations are based on the Lennard-Jones potential with energy scale  $\epsilon$  and length scale  $\sigma$ ,  $v(x = r/\sigma) = 4\epsilon(x^{-12} - x^{-6})$ , which is often used as a prototypical small-molecule potential and as a basis for modeling both noble gases and metals. The potential is truncated and shifted so as to go to zero at  $3\sigma$  as in our previous Letter [3,18,20]. The phase diagram then includes vapor, liquid, and solid phases with a liquid-vapor critical point and vapor-liquid-solid triple points (which are different for different crystal polymorphs [19]). For LJ, the minimum

TABLE I. Fluid-solid interfacial and coexistence properties for the hard-spheres system. The physical quantities reported are the fluid and solid densities, the pressure, the chemical potential, and the fluid-solid interfacial free energies for multiple faces of the fcc solid, except for the last two rows reporting cDFT results for bcc. The rows reporting values from this Letter are marked by an asterisk.

Source	$\rho_f \sigma^3$	$\rho_s \sigma^3$	$\beta P \sigma^3$	$\beta \mu$	$\beta \gamma_{(001)} \sigma^2$	$\beta \gamma_{(110)} \sigma^2$	$\beta \gamma_{(111)} \sigma^2$
WBII (Härtel <i>et al.</i> [9])	0.945	1.039	11.87	16.38	0.69	0.67	0.64
*WBII ( $\Delta \approx 0.0125\sigma$ )	0.946	1.039	11.94	16.46	...	...	...
*WBII ( $\Delta \approx 0.025\sigma$ )	0.950	1.041	12.16	16.68	0.69	...	...
*WBII ( $\Delta \approx 0.05\sigma$ )	0.966	1.046	13.09	17.65	0.71	...	...
*esFMT ( $\Delta \approx 0.05\sigma$ )	0.942	1.027	11.96	16.50	0.51	0.47	0.46
Simulation (Davidchack [8])	0.940	1.041	...	...	0.58	0.56	0.54
Simulation (Härtel <i>et al.</i> [9])	0.938	1.039	...	...	0.63	0.61	0.60
bcc WBII (Turci <i>et al.</i> [26])	1.016	1.045	...	...	0.34	0.33	0.32
*bcc esFMT ( $\Delta \approx 0.05\sigma$ )	0.967	1.008	13.45	18.06	0.21	0.20	0.20

free-energy solid phase is either fcc or hcp, depending on the conditions [28], but there is little difference between their free energies [18]. We chose to work with the fcc phase out of convenience and because there are more simulation results for this phase.

Below, to check plausibility, we compare our results to simulation when possible, and to reduce the effect of differences in details of how the potential is cut off [29], the temperature is scaled to the triple point temperature (for fcc or bcc as appropriate and denoted  $k_B T_{\text{fcc}}^* = 0.798\epsilon$  and  $k_B T_{\text{bcc}}^* = 0.742\epsilon$ , or generically  $T_{\text{xcc}}^*$ ) determined from the underlying method (e.g., cDFT or simulation). The chemical potential will be expressed in terms of the supersaturation  $S(T) \equiv (\mu - \mu_{\text{coex}})/k_B T$ , where  $\mu_{\text{coex}}$  is the chemical potential for coexistence (at the given temperature) of the two phases of the interface. For low-density vapors this is almost the same as the log of the ratio of the density to the coexisting density or the pressure to the coexisting pressure, but this does not, of course, hold for the liquid. Finally, for the vapor phase, we have also performed exact, zero-temperature calculations whereby the free energy is simply replaced by the internal energy and the vapor density is zero [19].

The surface free energies from our calculations for solid-liquid interfaces are shown in Fig. 2. For the fcc phase, the ordering of the surface tensions is  $\gamma_{(111)} < \gamma_{(110)} < \gamma_{(001)}$ , the same as found for hard spheres above. Note, however, that the difference between the surface tensions goes to zero near the triple point and grows as the temperature increases, although it is never very large in the range of temperatures considered here. Figure 2 also includes simulation data from Laird *et al.* [30] and shows that the values obtained are physically reasonable.

For the bcc phase, one sees that at all temperatures the interfacial free energy is roughly half that of the fcc phase,

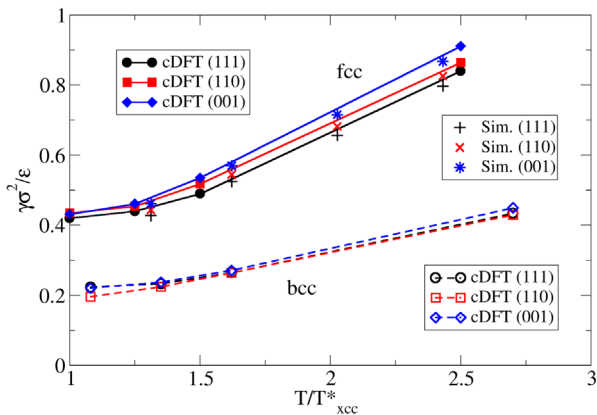


FIG. 2. Interfacial free energies for the liquid-solid coexistence in simple fluids. The temperatures are scaled using the corresponding triple point temperature:  $T_{\text{fcc}}^*$  or  $T_{\text{bcc}}^*$ . The simulation data come from Laird *et al.* [30]. Error bars are a bit smaller than the symbols, not taking the finite spacing  $\Delta$  into account (see Ref. [19] for details).

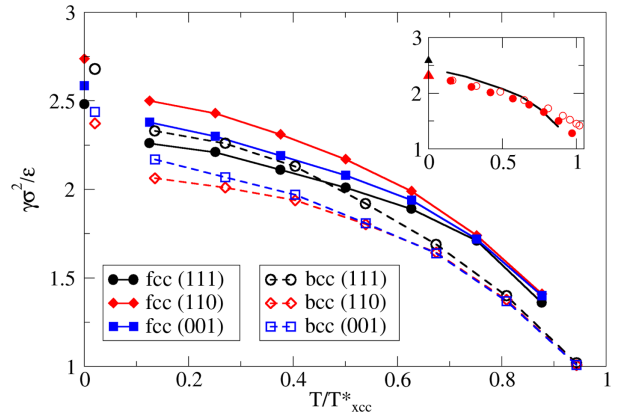


FIG. 3. Same as Fig. 2 for vapor-solid coexistence. The zero-temperature values are the exact calculations and for bcc are offset on the temperature axis, for clarity. The inset shows the fcc (001) results compared to the simulation data of Broughton and Gilmer [31] and Tipseev *et al.* [32].

suggesting that the bcc structure is energetically more favorable than fcc for small clusters as will be discussed below. The bcc values show very little difference between the different crystal planes, although in fact  $\gamma_{(110)} < \gamma_{(111)} < \gamma_{(001)}$ . To our knowledge, there are no studies reporting liquid-bcc interfacial free energies from simulation.

Interfacial free energies for solid-vapor interfaces are shown in Fig. 3 together with simulation results. The fcc results are again in reasonable agreement with the available simulation values showing they are physically plausible, although the temperature dependence of the cDFT results are somewhat stronger near the triple point than observed in simulation. The simulation data come from two references that use different techniques. Extrapolation of our results to zero temperature differs somewhat from the exact results, also shown in Fig. 3, but this is likely due to the finite size of the computational grid [19].

For the bcc phase, we encountered the presence of an instability in the crystal structure when calculating  $\gamma_{(110)}$  and  $\gamma_{(111)}$ . Our zero-temperature calculations confirmed previous observations [15,33] that the bulk bcc phase (for LJ) is unstable with respect to displacement of the (110) plane leading to distortions of the bulk crystal when calculating these surface tensions. These zero-temperature calculations show that the system is unstable to transformation to an hcp lattice. Our cDFT calculations confirmed that the instability persists at finite temperatures up to the triple point. In order to calculate the surface tension in this case, it was necessary to freeze the bulk solid and to only relax the planes near the interface [19]. Importantly, no such instability was found for the bcc-liquid interface [19].

*Polymorphic behavior.*—The capillary model used in classical nucleation theory (CNT) (assuming uniform bulk phases inside and outside a spherical cluster and an infinitely thin interface) results in the standard CNT expression for the excess free energy of a cluster [1,34],

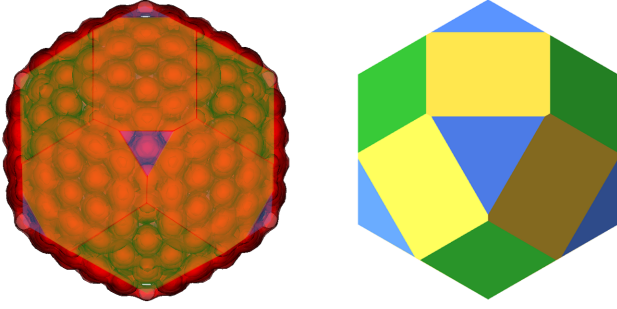


FIG. 4. Left: example of bcc cluster generated by freezing a droplet of liquid in a vapor background, in a cDFT calculation [37]. Right: Wulff construction using the interfacial free energies obtained from cDFT calculations. The yellow, green, and blue facets are (110), (001), and (111), respectively. The image on the left is an orthogonal projection generated using visIt [38], while the one on the right was produced using WULFFPACK [36].

$\Delta\Omega = \frac{4}{3}\pi R^3 \Delta\omega_{s-f} + 4\pi R^2 \gamma_{s-f}$ , where  $\Delta\omega_{s-f}$  is the free-energy difference between the solid and fluid per unit volume,  $R$  is the radius of the cluster, and  $\gamma_{s-f}$  is the effective surface tension (a weighted average of the values for the various faces). The radius  $R_c = -2\gamma_{s-f}/\Delta\omega_{s-f}$  for which the derivative of  $\Delta\Omega$  vanishes is the critical radius in classical nucleation theory and the value of the excess free energy is the CNT barrier [1]. A more extended presentation of the capillary model and its use is given in the Supplemental Material [22].

We tested the capillary model by comparing it to clusters generated using cDFT [35] by freezing liquid droplets [20] and using the canonical-grand-canonical duality for critical clusters proven in Refs. [3,20]. An example of a perfect bcc cluster is shown in Fig. 4, together with the predicted zero-temperature equilibrium shape determined using our surface tensions and the WULFFPACK PYTHON package [36]. While the (110) plane dominates the structure in both cases, the smaller facets are replaced by rounded edges as one might expect at finite temperatures. Comparison of the excess free energies predicted by the capillary model and those of actual clusters generated by cDFT, see Fig. 5, confirm that, as crude as it is, the model gives quite reasonable values for both fcc and bcc structures. As expected, the capillary prediction using the lowest surface tension for each lattice is a hard lower bound on the cluster free energies since the real clusters contain a mixture of crystal faces, are not spherical, and also involve line tensions between the facets.

Using our surface tensions and bulk free energies, the capillary model predicts that bcc is more stable than fcc for small clusters and that this reverses for large clusters. The size of cluster (expressed as number of atoms) above which fcc becomes favored, i.e., the crossover size, as a function of temperature is shown in Fig. 6 (see also the Supplemental Material [22] where the state points presented in Fig. 6 are shown in the context of the phase

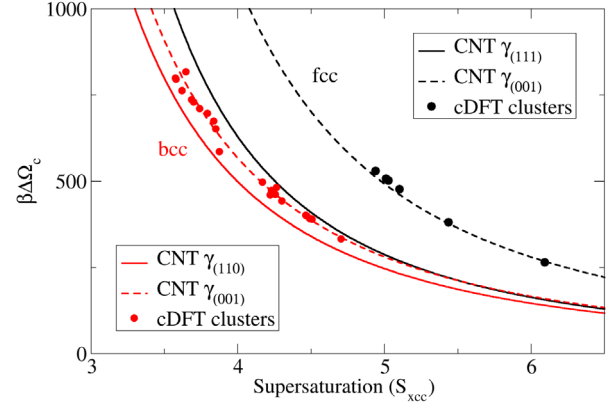


FIG. 5. Free-energy barriers of fcc (upper, black curves and symbols) and bcc (lower, red curves and symbols) clusters in a vapor background [37]. The full lines are the capillary model predictions using the smallest interfacial free energy for each structure, the dashed line is that using the second smallest. The dots are cDFT calculations of clusters generated by freezing a liquid droplet [20]. The temperature is  $k_B T/\epsilon = 0.3$ , which corresponds to  $T/T_{\text{bcc}}^* = 0.580$  for bcc and  $T/T_{\text{fcc}}^* = 0.546$  for fcc.

diagram) [37]. For crystallization from both melt and vapor, the maximal crossover size occurs near the triple points, although for the freezing, the variation with temperature is rather weak. In the case of the vapor background, the large crossover value near the triple point is due partly to an increase in the difference in surface tensions but mostly to the fact that the bulk free energies become very close at this temperature. This is consistent with the Alexander and McTague [14] result that bcc should be the first structure formed in the process of nucleation and with the observations of ten Wolde *et al.* [16] of predominantly bcc structure

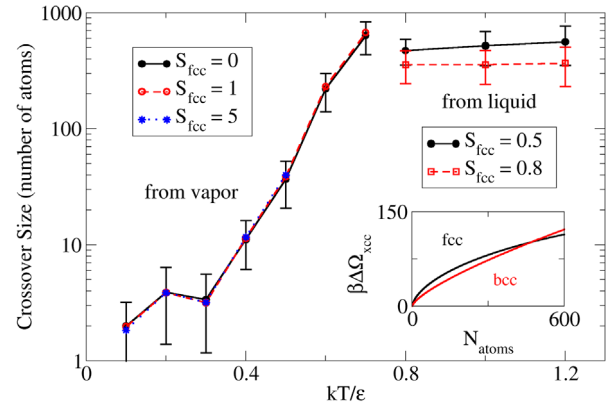


FIG. 6. bcc to fcc crossover cluster size as a function of temperature for the formation from the vapor and from the liquid. Error bars are mostly due to numerical uncertainties coming from the surface-tension calculations [19]. The inset shows an example of the crossover from bcc to fcc stability as a function of cluster size for  $k_B T/\epsilon = 0.8$  and  $S_{\text{fcc}} = 0.5$ . See the section “Bulk Thermodynamics” in the Supplemental Material [22] for a phase diagram showing the state points used here.



for small clusters and fcc at larger sizes with the crossover being for clusters of some hundreds of molecules. It is also helps explain their observation of fcc clusters with bcc surface layers: since the surface free energy of the bcc is about half that of the fcc, this is not surprising although one would have to also determine the bcc-fcc surface tension to prove that this is to be expected.

**Conclusions.**—Our Letter is not inconsistent with other recent ideas for understanding crystallization from the melt. For example, using simulations to map free-energy surfaces to probe the thermodynamics of polymorphs [39] is clearly quite similar in spirit since the ultimate goal is likewise based on the free-energy landscape. Similarly, the idea that local structure in supercooled liquids favors one polymorph over another as discussed by Russo and Tanaka [40] is not very different from the intuition that the lower surface free energy of one crystal structure compared to another must be related to a greater or lesser similarity between the local structure of the fluid at the interface and that of the crystal. Of course, nucleation is an inherently nonequilibrium process, and free energy is only one factor that, along with kinetics, determines the nucleation pathway [3,41].

For crystals forming from the vapor, or precipitating from a dilute solution, the bcc phase does have somewhat lower surface tension but it is unstable, rather than metastable, so any bcc clusters observed in this case can only be a transient stage that should eventually decay to the fcc or hcp structure. Finally, implications for hard spheres are discussed in the Appendix where it is noted that additional lattice structures complicate the picture.

We thank our colleague Yves Geerts for useful discussions. The work of C.S. was funded by the Belgian National Fund for Scientific Research (FRS-FNRS) under the FRIA grant FC 38825. The work of J.F.L. was supported by the European Space Agency (ESA) and the Belgian Federal Science Policy Office (BELSPO) in the framework of the PRODEX Programme, Contract No. ESA AO-2004-070.

**Appendix: Hard sphere polymorphism.**—For hard spheres, we find lower surface tension for the bcc phase than for the fcc phase (see Table I), and so one would expect that it would also be the case that small bcc clusters have lower free energy small fcc clusters and hence could play a role in crystallization. Indeed, we show in Fig. 7 the crossover size as a function of supersaturation. Yet, careful studies such as that of Auer and Frenkel [42] and Wöhler and Schilling [43] show no evidence that small clusters are preferentially bcc. It could simply be that kinetic factors are more important than thermodynamics in this case, but we also note that there are two differences from Lennard-Jones that complicate the question for hard spheres.

First, unlike for Lennard-Jones, we find that the crossover size for hard spheres decreases rapidly with

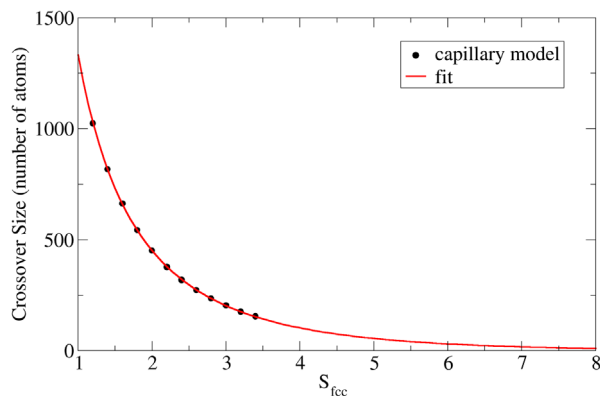


FIG. 7. bcc to fcc crossover cluster size as a function of supersaturation,  $S_{fcc}$  for crystallization of hard spheres. Note that  $3 \leq S_{fcc} \leq 8$  corresponds to the range of liquid packing fractions of  $0.5 \leq \eta \leq 0.548$ , where  $\eta = \pi \rho_f \sigma^3 / 6$ . The fit is to a function of the form  $f(x) = A \exp(-Bx)/x$  and only points with  $S_{fcc} \leq 2.5$  were used to determine the constants. The extrapolated crossover size for  $S_{fcc} = 8$  is about 11 atoms.

supersaturation. Since most, if not all, freezing studies in hard spheres are done at relatively high supersaturation [43], it may be that the crossover size is very small. Indeed, for a fluid packing fraction of 0.52, which is at the lower end of simulation and experimental studies, we estimate the crossover size to be about 150 atoms. Given that our calculations are not exact, the actual figure could be lower. Furthermore, the rapid decrease with supersaturation means that the crossover size at higher supersaturations is so small that differences of structure become ambiguous.

A second factor is that in hard spheres it is neither fcc nor bcc that dominates but rather hcp with random stacking faults [42] (referred to as rhcp), so that it could simply be that this structure is even more favored than bcc. Resolving this would require much more extensive calculations.

\*jlutsko@ulb.ac.be

- [1] D. Kashchiev, *Nucleation: Basic Theory with Applications* (Butterworth-Heinemann, Oxford, 2000).
- [2] P. G. Vekilov, *Nonclassical nucleation, Crystallization via Nonclassical Pathways Volume 1: Nucleation, Assembly, Observation & Application* (American Chemical Society, Washington, 2020), Chap. 2, pp. 19–46.
- [3] J. F. Lutsko, How crystals form: A theory of nucleation pathways, *Sci. Adv.* **5**, eaav7399 (2019).
- [4] D.-K. Bučar, R. W. Lancaster, and J. Bernstein, Disappearing polymorphs revisited, *Angew. Chem., Int. Ed. Engl.* **54**, 317 (2008).
- [5] L. L. Zhang, S. Yang, W. Wei, and X. J. Zhang, Genetic polymorphisms affect efficacy and adverse drug reactions of DMARDs in rheumatoid arthritis, *Pharmacogenet. Genomics* **24**, 531 (2014).
- [6] S. L. Morissette, S. Soukasene, D. Levinson, M. J. Cima, and Ö. Almarsson, Elucidation of crystal form diversity of the HIV protease inhibitor ritonavir by high-throughput

- crystallization, *Proc. Natl. Acad. Sci. U.S.A.* **100**, 2180 (2003).
- [7] W. Cabri, P. Ghetti, G. Pozzi, and M. Alpegiani, Polymorphisms and patent, market, and legal battles: Cefdinir case study, *Org. Process. Res. Dev.* **11**, 64 (2007).
- [8] R. L. Davidchack, Hard spheres revisited: Accurate calculation of the solid–liquid interfacial free energy, *J. Chem. Phys.* **133**, 234701 (2010).
- [9] A. Härtel, M. Oettel, R. E. Rozas, S. U. Egelhaaf, J. Horbach, and H. Löwen, Tension and Stiffness of the Hard Sphere Crystal-Fluid Interface, *Phys. Rev. Lett.* **108**, 226101 (2012).
- [10] R. Evans, The nature of the liquid-vapour interface and other topics in the statistical mechanics of non-uniform, classical fluids, *Adv. Phys.* **28**, 143 (1979).
- [11] J. F. Lutsko, Recent developments in classical density functional theory, *Adv. Chem. Phys.* **144**, 1 (2010).
- [12] M. Oettel, S. Görig, A. Härtel, H. Löwen, M. Radu, and T. Schilling, Free energies, vacancy concentrations, and density distribution anisotropies in hard-sphere crystals: A combined density functional and simulation study, *Phys. Rev. E* **82**, 051404 (2010).
- [13] J. F. Lutsko, Explicitly stable fundamental-measure-theory models for classical density functional theory, *Phys. Rev. E* **102**, 062137 (2020).
- [14] S. Alexander and J. McTague, Should All Crystals be bcc? Landau Theory of Solidification and Crystal Nucleation, *Phys. Rev. Lett.* **41**, 702 (1978).
- [15] W. C. Swope and H. C. Andersen,  $10^6$ -particle molecular-dynamics study of homogeneous nucleation of crystals in a supercooled atomic liquid, *Phys. Rev. B* **41**, 7042 (1990).
- [16] P. R. ten Wolde, M. J. Ruiz-Montero, and D. Frenkel, Numerical Evidence for bcc Ordering at the Surface of a Critical fcc Nucleus, *Phys. Rev. Lett.* **75**, 2714 (1995).
- [17] C. Desgranges and J. Delhommelle, Controlling Polymorphism during the Crystallization of an Atomic Fluid, *Phys. Rev. Lett.* **98**, 235502 (2007).
- [18] J. F. Lutsko and C. Schoonen, Classical density-functional theory applied to the solid state, *Phys. Rev. E* **102**, 062136 (2020).
- [19] C. Schoonen and J. F. Lutsko, companion paper, Using classical density functional theory to determine crystal-fluid surface tensions, *Phys. Rev. E* **106**, 064110 (2022).
- [20] J. F. Lutsko and J. Lam, Classical density functional theory, unconstrained crystallization, and polymorphic behavior, *Phys. Rev. E* **98**, 012604 (2018).
- [21] J. Guérolé, W. G. Nöhring, A. Vaid, F. Houllé, Z. Xie, A. Prakash, and E. Bitzek, Assessment and optimization of the fast inertial relaxation engine (FIRE) for energy minimization in atomistic simulations and its implementation in LAMMPS, *Comput. Mater. Sci.* **175**, 109584 (2020).
- [22] See Supplemental Material at <http://link.aps.org/supplemental/10.1103/PhysRevLett.129.246101> for full technical details of the cDFT model, thermodynamic data, error estimates, and additional calculations, which includes Refs. [23,24].
- [23] R. Shuttleworth, The surface tension of solids, *Proc. Phys. Soc. London Sect. A* **63**, 444 (1950).
- [24] N. Di Pasquale and R. L. Davidchack, Shuttleworth equation: A molecular simulations perspective, *J. Chem. Phys.* **153**, 154705 (2020).
- [25] M. Oettel, S. Dorosz, M. Berghoff, B. Nestler, and T. Schilling, Description of hard-sphere crystals and crystal-fluid interfaces: A comparison between density functional approaches and a phase-field crystal model, *Phys. Rev. E* **86**, 021404 (2012).
- [26] F. Turci, T. Schilling, M. H. Yamani, and M. Oettel, Solid phase properties and crystallization in simple model systems, *Eur. Phys. J. Special Topics* **223**, 421 (2014).
- [27] G. Grimvall, B. Magyari-Köpe, V. Ozoliņš, and K. A. Persson, Lattice instabilities in metallic elements, *Rev. Mod. Phys.* **84**, 945 (2012).
- [28] A. Travesset, Phase diagram of power law and Lennard-Jones systems: Crystal phases, *J. Chem. Phys.* **141**, 164501 (2014).
- [29] P. Grosfils and J. F. Lutsko, Dependence of the liquid-vapor surface tension on the range of interaction: A test of the law of corresponding states, *J. Chem. Phys.* **130**, 054703 (2009).
- [30] B. B. Laird, R. L. Davidchack, Y. Yang, and M. Asta, Determination of the solid-liquid interfacial free energy along a coexistence line by Gibbs-Cahn integration, *J. Chem. Phys.* **131**, 114110 (2009).
- [31] J. Q. Broughton and G. H. Gilmer, Molecular dynamics investigation of the crystal-fluid interface. IV. Free energies of crystal-vapor systems, *J. Chem. Phys.* **84**, 5741 (1986).
- [32] J. P. Tipseev A. O. Rino and E. D. Zanotto, Direct determination of Lennard-Jones crystal surface free energy by a computational cleavage method, *J. Chem. Phys.* **155**, 094101 (2021).
- [33] N. Krainyukova, On the mechanism of the BCC-HCP transformations in small Lennard-Jones crystals, *J. Low Temp. Phys.* **150**, 317 (2008).
- [34] J. F. Lutsko, Density functional theory of inhomogeneous liquids. III. Liquid-vapor nucleation, *J. Chem. Phys.* **129**, 244501 (2008).
- [35] For practical reasons, the calculations involving clusters were performed on a coarser lattice ( $\Delta = 0.2\sigma$ ) than used elsewhere in this Letter. For the construction of Fig. 5 all surface tensions were recalculated using the coarser lattice. Details can be found in Refs. [19,22].
- [36] J. M. Rahm and P. Erhart, WulffPack: A Python package for Wulff constructions, *J. Open Source Software* **5**, 1944 (2020).
- [37] For these calculations, we used our best values of the thermodynamic properties based on the smallest computational lattice spacing.
- [38] H. Childs *et al.*, VisIt: An end-user tool for visualizing and analyzing very large data, in *High Performance Visualization: Enabling Extreme-Scale Scientific Insight*, edited by E. Bethel, H. Childs, and C. Hansen (Taylor & Francis, Boca Raton, FL, 2013), pp. 357–372.
- [39] P. M. Piaggi and M. Parrinello, Predicting polymorphism in molecular crystals using orientational entropy, *Proc. Natl. Acad. Sci. U.S.A.* **115**, 10251 (2018).

- [40] J. Russo and H. Tanaka, Selection mechanism of polymorphs in the crystal nucleation of the Gaussian core model, *Soft Matter* **8**, 4206 (2012).
- [41] L.O. Hedges and S. Whitlam, Limit of validity of Ostwald's rule of stages in a statistical mechanical model of crystallization, *J. Chem. Phys.* **135**, 164902 (2011).
- [42] S. Auer and D. Frenkel, Prediction of absolute crystal-nucleation rate in hard-sphere colloids, *Nature (London)* **409**, 1020 (2001).
- [43] W. Wöhler and T. Schilling, Hard Sphere Crystal Nucleation Rates: Reconciliation of Simulation and Experiment, *Phys. Rev. Lett.* **128**, 238001 (2022).